Nuclear Materials and Energy 41 (2024) 101778

Contents lists available at ScienceDirect

Nuclear Materials and Energy

journal homepage: www.elsevier.com/locate/nme

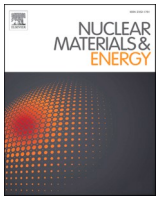

Properties of boron layers deposited during boronisations in W7-X

M. Mayer [a,*], M. Balden [a], T. Bräuer [b], D. Cipciar [b], C.P. Dhard [b], P. Drews [c], S. Elgeti [a], D. Höschen [c], C. Killer [b], D. Naujoks [b], N. Sandri [c], J.-H. Schmid-Dencker [a], L. Vanó [b], H. Viebke [c], O. Volzke [b], W7-X Team [1]

[a] Max-Planck-Institut für Plasmaphysik, Garching, Germany
[b] Max-Planck-Institut für Plasmaphysik, Greifswald, Germany
[c] Forschungszentrum Jülich, Jülich, Germany

ARTICLE INFO

Keywords:
W7-X
Boronisation
Wall conditioning
Ion beam analysis
Multi-purpose manipulator

ABSTRACT

Boronisation was first used for wall conditioning in W7-X during the OP 1.2b operational period, which was characterized by the use of the fine-grain graphite Test Divertor Unit (TDU) and inertial cooling only. After this period, deposited layers were observed on all inner surfaces. Deposited layers were analyzed on 21 inner wall tiles using ion beam analysis methods, the deposited layers consisted mostly of boron with additional carbon and oxygen. During the operational period OP 2.1 with an actively water cooled divertor made of carbon fiber reinforced carbon, different materials were exposed during two individual boronisations using the multi-purpose manipulator. Deposited boronisation layers on the samples were analyzed using nuclear reaction analysis. The deposited layer thicknesses showed some variation depending on substrate material and surface roughness, but a systematic dependence on material and/or roughness was not observed. Under the typical boronisation conditions at W7-X, one A × h (Ampere times hour) of boronisation results in a boronisation layer with a thickness of about 30 ± 15 × 10^{15} B-atoms/cm^2 (about 3 ± 1.5 nm) at the position of the multi-purpose manipulator. The oxygen gettering capacity of the layers is up to 0.5 – 0.9O/B.

1. Introduction

Wendelstein 7-X (W7-X) [1–6] is an advanced stellarator with superconducting coils. During the second operational phase OP 1.2 a divertor, the so-called Test Divertor Unit (TDU) [7,8], consisting of adiabatically-cooled fine-grain graphite tiles, was used. OP 1.2 was subdivided in two sub-phases: OP 1.2a in the year 2017 and OP 1.2b in the year 2018. During OP 1.2a wall conditioning was performed by baking and glow-discharge cleaning in H and He, but without boronisations [9]. This resulted in high levels of oxygen and carbon impurities in the plasma with Z_{eff} (as obtained from bremsstrahlung measurements) up to values of 4.5 in reference discharges [10]. Oxygen originated from thermal outgassing of water molecules from the internal surfaces of carbon components, resulting in a high erosion of carbon especially at the divertor strike line [11]. The high oxygen and carbon concentrations in the plasma limited the operational window of the machine and prevented operation at high core densities due to the reduced radiation-induced density limit [10].

In order to reduce this high impurity content, three boronisations were applied in OP 1.2b. This resulted in a substantial decrease of the oxygen and carbon concentrations in the plasma [10,12]. After the first boronisation the oxygen to hydrogen flux ratio at the divertor decreased by a factor of ten, while the carbon to hydrogen flux decreased by a factor of four [10]. With subsequent boronisations the O levels in the plasma decreased further. The lowest values in this period were achieved after the third boronisation and were more than a factor of 100 lower than before the boronisations. This decrease of the impurity concentration significantly extended the operational window of W7-X. The line-integrated electron density increased from 4 × 10^{19} m^{-2} to above 1 × 10^{20} m^{-2} and the diamagnetic energy increased from 330 kJ to 510 kJ [10]. Z_{eff} decreased to values of about 1.2 in reference discharges. Boronisations therefore proved to be a key element in achieving good plasma performance.

During the years 2019 – 2021 the water-cooled steady-state divertor consisting of carbon-fiber-composite (CFC) tiles was installed. This divertor has the same shape as the TDU. Having demonstrated the need

* Corresponding author.
E-mail address: matej.mayer@ipp.mpg.de (M. Mayer).
[1] See the author list in T. Sunn Pedersen et al Nucl. Fusion 62 (2022) 042022.

https://doi.org/10.1016/j.nme.2024.101778
Received 5 July 2024; Received in revised form 26 September 2024; Accepted 15 October 2024
Available online 16 October 2024

for boronisation in OP 1.2, boronisation was continued in OP 2.1. This operational period took place in the year 2022 and was the first with the water-cooled CFC divertor.

Based on the observed importance of boronisations for good plasma performance in W7-X, more information on the properties of boronisation layers in W7-X is highly desired. This work presents measurements of deposited layers observed after the operational period OP 1.2b at various places inside the machine, and of layers deposited on samples exposed during individual boronisations with the multi-purpose manipulator (MPM) during OP 2.1. This allows us to obtain information on the composition, thickness, lateral distribution, and oxygen gettering capacity of these layers and allows to compare layer properties during individual boronisations with campaign-integrated data.

2. Experimental

2.1. Boronisations in W7-X

Three boronisations were performed during OP 1.2b, the time lag between individual boronisations was about 3000 plasma seconds. Boronisations were performed in a glow discharge in helium (He-GD) with 90 % He and 10 % B_2H_6 with the vessel walls at room temperature. In OP 1.2b this procedure was conducted three times with 45, 84 and 68 bar * l (bar times liter) of He-B_2H_6 mixture during 3.5, 5.5 and 5 h, respectively [10]. Typically 7 to 9 glow discharge electrodes were used, the electrode voltages were 330 – 430 V at gas pressures in the range 4.5 – 8.5 $\times$ 10^{-3} mbar. Assuming boron is equally deposited on the inner walls, all injected boron ends up on the wall, and assuming an inner wall area of 110 m^2, this leads to an indicative thickness value of 10–24 nm for the individual boronisations in OP 1.2b [9,13]. It should be noted, that more recent work [14] derived a total wall area inside W7-X of 192.5 m^2. This will be discussed further in section 3.1.

Five boronisations were performed in OP 2.1 with 46, 6, 35.4, 38.1, and 48 bar*l during 2:20, 2, 2:26, 3:10 and 3:09 h, respectively. The electrode voltages were 310 – 490 V at a current of 0.9 – 1.7 A and gas pressures in the range 4 – 11 $\times$ 10^{-3} mbar. Before boronisation the walls were sometimes cleaned with glow discharge cleaning in 60 % He and 40 % H_2.

Boronisations are labeled starting with one for the first boronisation in a campaign. In this work, we will usually use the date of the boronisation.

2.2. Samples and analysis methods

2.2.1. Inner wall tiles in OP1.2b

21 W-coated fine-grain graphite tiles were exposed during OP 1.2b at the inner heat shield at several positions, see Fig. 1 (taken from [15]) for a representation of tile positions. The initial W layer thickness was in the range between 90 and 200 nm, as derived from Elastic Backscattering Spectrometry (see below), and allowed to separate deposited B, C and O from the bulk substrate material. The tiles were analyzed after exposure in OP 1.2b using Elastic Backscattering Spectrometry (EBS) [16] at the IPP tandem accelerator facility in the Bombardino chamber using the BesTec flange [17] with incident protons at an energy of 2.5 MeV at a scattering angle of 165° and normal incidence. A passivated implanted planar silicon detector (PIPS® detector) with a nominal energy resolution of about 12 keV and a thickness of 300 μm was used. The measured spectra were simulated with the program SIMNRA [18] with SRIM [19] stopping powers and non-Rutherford scattering cross-sections from SigmaCalc for light elements [20]. A typical spectrum and the corresponding simulation are shown in Fig. 2. Typically, a thin layer consisting of B, C and O with traces of N has been deposited on top of the W coating. The deposited layer probably also contains hydrogen, which is not visible with the applied methods. Due to the W-coating, deposited carbon and the contribution of the bulk carbon can be separated. The thickness of the W coating did not change within the accuracy of the applied methods. Oxygen is present in the deposited layer, but also in the W coating at a level of a few %. These two oxygen contributions cannot be separated in the spectra. Because the tiles were analyzed before exposure in W7-X, the amount of oxygen in the W coatings is known and was subtracted from the integral amount of oxygen in order to get the amount of oxygen in the deposited layer. The measured spectra and the simulations generally agree well, except for the tail of the W peak in channels 675–700. This tail can be explained by the deep open pores at the surface of fine-grain graphite: The interior of these pores gets also coated with W and results in distortions of the spectrum like long tails towards lower energies. This very special surface structure cannot be fully represented by the surface roughness model of SIMNRA.

2.2.2. Samples exposed with multi-purpose manipulator

Eight samples each were exposed with the multipurpose manipulator (MPM) during two boronisations in OP 2.1 (3rd boronisation on 4.2.2023 and 4th boronisation on 25.2.2023), a photo of the manipulator probe head with mounted samples is shown in Fig. 3. Sample dimensions are 12 $\times$ 10 $\times$ 5 mm^3. The samples were exposed during the whole boronisation and transported through air before measurements. The time lag between exposure and measurement was 1 week (3rd boronisation) and 3 weeks (4th boronisation), respectively. The samples were exposed behind the last closed flux surface. The samples were analyzed after exposure with incident 3 MeV $^3He^+$ ions using nuclear reaction analysis (NRA) [21] employing the reactions $^{10}B(^3He,p_{0,1})^{12}C$, $^{11}B(^3He,p_0)^{13}C$, $^{12}C(^3He,p_{0,1,2})^{14}N$ and $^{16}O(^3He,p_0)^{18}F$ using cross-section data from [22,23,24]. Two different detectors both located at reaction angles of 135° were used. One detector was a PIPS detector with a surface area of 300 mm^2, a depletion depth of 2000 μm and a solid angle of 30.6 msr. It is covered with a 5 μm Ni and 12 μm Mylar foil in order to stop backscattered ^3He ions. The second detector is a lithium drifted silicon detector Si(Li) for charged particles detection with a surface area of 500 mm^2, a useful thickness of 2000 μm and a solid angle of 78.7 msr. It is covered with a 50 μm Mylar foil. Both detectors have apertures with parabolic shapes in order to minimize geometrical straggling [25].

A typical NRA spectrum is shown in Fig. 4. The reactions $^{10}B(^3He, p_1)^{12}C$ and $^{11}B(^3He,p_0)^{13}C$ are used for detection of boron, the reactions $^{12}C(^3He,p_0)^{14}N$ and $^{12}C(^3He,p_2)^{14}N$ for detection of ^{12}C, and the reaction $^{16}O(^3He,p_0)^{18}F$ for the detection of ^{16}O. Protons from the $^{12}C(^3He, p_1)^{14}N$ and $^{16}O(^3He,p_0)^{18}F$ reactions partly overlap. In order to take this overlap into account, the number of protons was calculated from the known cross-section of the $^{12}C(^3He,p_1)^{14}N$ reaction and subtracted from the oxygen signal. Due to the very small cross-section of $^{12}C(^3He,p_1)^{14}N$ at this energy, the contribution of protons from the ^{12}C reaction is typically only 5–10 % of the oxygen signal. The background in channels below about 400 was taken into account by linear interpolation between the values to the left and right of the peak of interest.

3. Results and discussion

3.1. Inner wall after OP 1.2b

Photos of two different inner wall tiles after exposure in OP 1.2b are shown in Fig. 5 and Fig. 6. The tiles were coated with a W layer and initially showed a metallic shiny impression. After exposure both tiles were coated more or less homogeneously with a deposited layer. The tiles were analyzed using EBS with 2.5 MeV protons, see section 2.2.1. In the case of TH-Y069 (Fig. 5) the layer consists of boron, oxygen and carbon. The amount of boron is about 600 $\times$ 10^{15} B-atoms/cm^2 (about

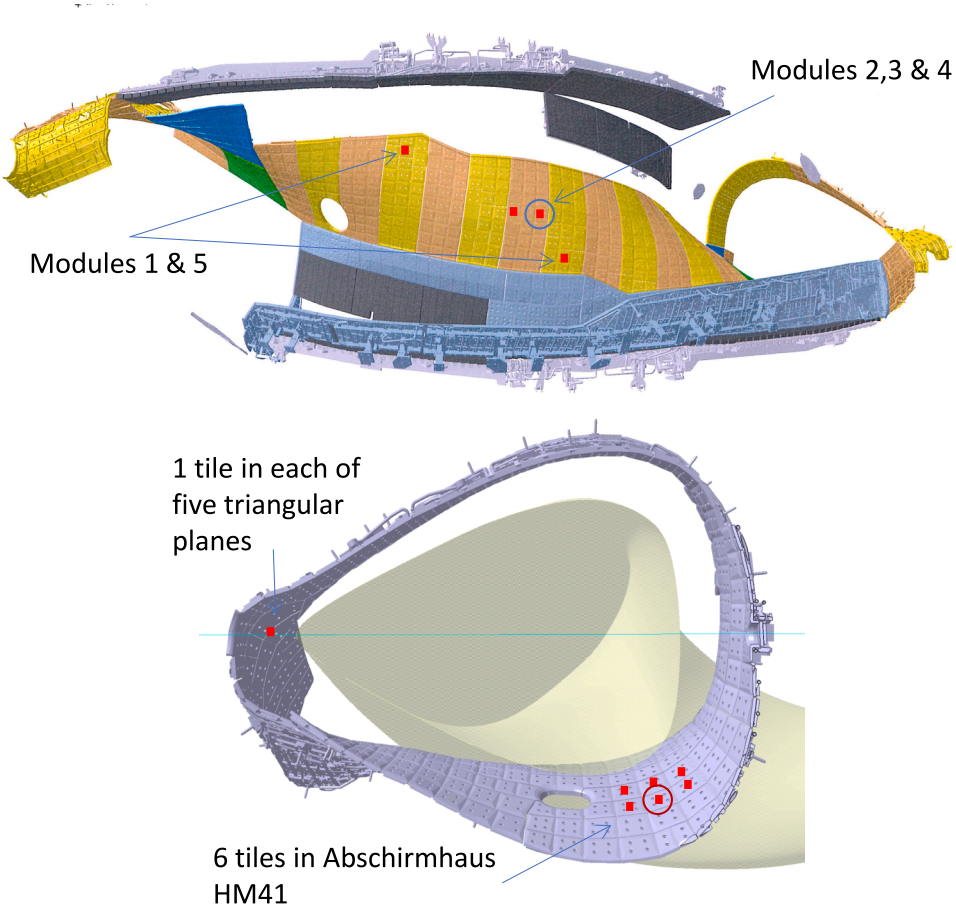

Fig. 1. Positions of the 21 inner heat shield tiles exposed in OP 1.2b. Modified from [15], the original figure has license CC BY 4.0, see https://creativecommons.org/licenses/by/4.0/. Tile TH-Y069 is marked with a red circle and is shown in Fig. 5. Tile TH-Z366 from module 2 is marked with a blue circle and is shown in Fig. 6.

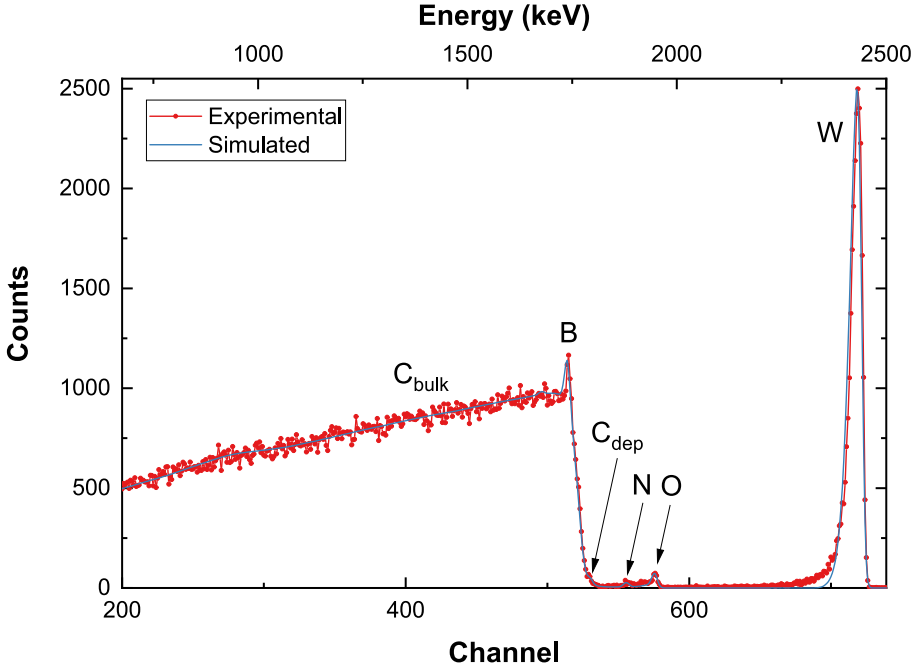

Fig. 2. Typical backscattering spectrum of a W-coated inner wall tile after OP 1.2b, measured with 2.5 MeV incident protons. Tile TH-Y069, analysis point in the middle of the tile, see Fig. 5. C_{dep} is the contribution of carbon deposited on top of the W layer, C_{bulk} is the contribution from the bulk carbon below the W layer.

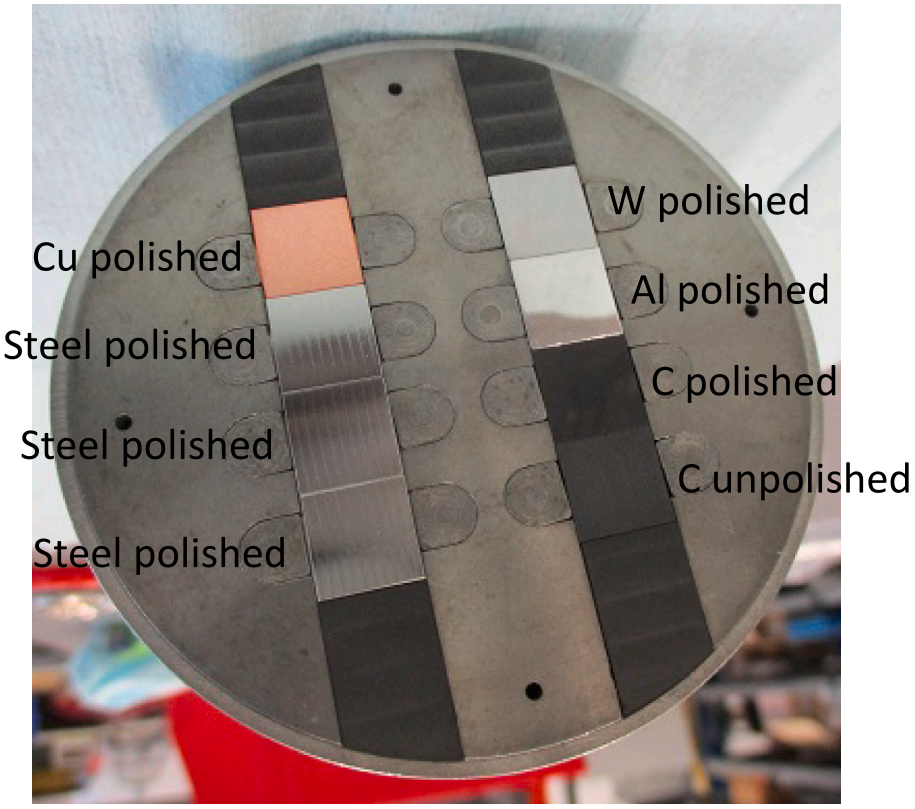

Fig. 3. Photo of the multi-purpose manipulator probe head with mounted samples for the boronisation on 4.2.2023. The steel samples belonged to a different experiment and were not analyzed in the framework of this investigation.

60 nm^2) with only minor variation along the surface of the tile, the O/B ratio is about 0.15. In the case of TH-Z366 (Fig. 6), the amount of boron is 100–200 $\times$ 10^{15} B-atoms/cm^2 (about 10 - 20 nm). The deposited layer contains more carbon, probably because the tile was between two vertical divertors, see Fig. 1.

Overall, the amount of boron on the 21 analyzed inner wall tiles was in the range 100 – 600 $\times$ 10^{15} B-atoms/cm^2 (about 10 - 60 nm). Most tiles were coated with a boron-rich layer mixed with carbon. The C/B ratio was in the range from above 0.15 – 0.5, although also more carbon-rich films were observed at some positions (see Fig. 6). For the boron-rich layers the O/B ratio varied over a large range of 0.15 – 0.92, with a tendency for thicker layers to show a lower O/B ratio. As the layers have been exposed to air prior to analysis, the oxygen most probably originates from the air exposure. Nevertheless, the amount of trapped oxygen allows to estimate the oxygen gettering capacity of the boronisation layers. This will be discussed in more detail in section 3.2. The lower O/B ratio of thicker layers might indicate, that oxygen is trapped only in a thinner surface layer and not homogeneously in the whole film thickness. However, the limited depth resolution of the applied methods, the rough technical surfaces, and the scatter of the data prevent a clear conclusion about the distribution and uptake of oxygen in the layers.

The variation of the amount of boron in the range 100 – 600 $\times$ 10^{15} B-atoms/cm^2 (about 10 - 60 nm) is in good agreement with colorimetry measurements of deposited layers on stainless-steel first wall panels inside W7-X after OP 1.2b, where deposited layers with thicknesses between 10 and 50 nm were observed [26]. Goriaev estimated in [9,13] average layer thicknesses of 10, 24, and 18 nm for the three boronisations in OP 1.2b based on the parameters of the boronisation discharges assuming an inner wall area of 110 m^2 and homogeneous deposition on the whole inner wall surface. This would result in a total boronisation layer thickness of 52 nm in OP 1.2b. Using the more recent value of 192.5 m^2 for the inner wall area [14], this gives an average layer thickness of 30 nm, which is in very good agreement with the ion beam analysis measurements and colorimetry. This demonstrates, that the methods presented in [9,13] are well suited to correctly predict the average layer thickness deposited during a boronisation.

It can be concluded, that a large fraction of the inner wall in W7-X was coated with a boron-rich layer of 10 – 60 nm after OP 1.2b. However, thicker deposits were observed at one glow discharge electrode, and localized thicker deposits in close vicinity of these electrodes or near gas inlets could be present. On areas with higher particle fluxes (such as divertor or baffle surfaces or limiters), such thin layers are quickly either eroded or covered by redeposited layers, so that such areas usually exhibit different compositions. Carbon erosion up to several μm has been observed at the TDU strike line [27], so that thin boronisation layers are expected to erode quickly at these areas. Redeposition of carbon up to several μm has been observed at some other areas of the TDU [27] and on baffle tiles. These redeposited layers typically contain also minor amounts of boron.

The amount of boron observed at a specific location after a whole operational period depends on the amount of boron deposited by boronisations during that campaign, but also on the amount of erosion by plasma ions and/or charge-exchange (CX) neutral particles. One can expect, that the thickness of boronisation layers depends on the distance to the next glow-discharge electrode active during the boronisation, the distance to the gas inlet, and the local geometry. On the scale of an individual wall tile with lateral dimensions of 5 – 10 cm the deposition therefore should be more or less uniform, unless the tile has a strong

[2] For conversion from atoms/cm^2 to nm we assume an atomic density of 1×10^{23} atoms/cm^3 for deposited layers. Because the density of deposited layers can vary over a wider range and is generally not well known, layer thicknesses in nm are only approximate and are given only for convenience of the reader.

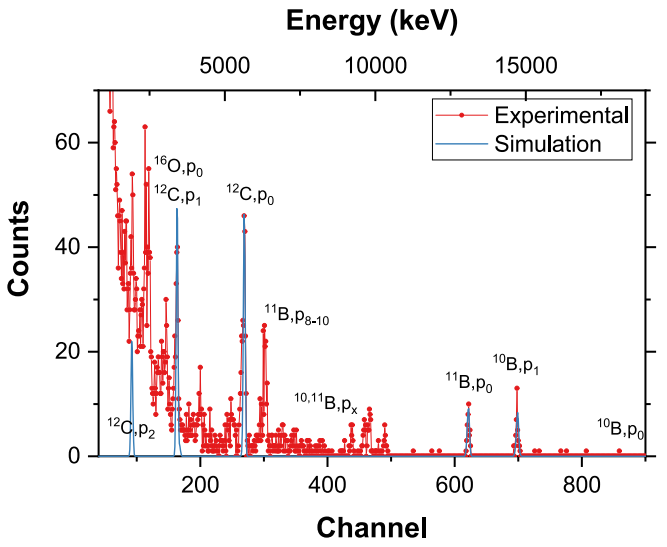

Fig. 4. Typical proton spectrum measured with incident 3000 keV ^{3}He ions at a reaction angle of 135° in the PIPS detector. The substrate was bulk W. Red dots: Experimental spectrum; blue line: Simulation using the SIMNRA code. The reaction ^{10}B(^{3}He,p$_0$)^{12}C (labeled in the figure as ^{10}B,p$_0$) has the highest energetic protons, but the cross-section is so low that less than one count is expected. The reactions ^{10}B(^{3}He,p$_1$)^{12}C and ^{11}B(^{3}He,p$_0$)^{13}C (labeled as ^{10}B,p$_1$ and ^{11}B,p$_0$) are visible as separated peaks. In the regions 290 – 500 channels and 100 – 140 channels additional peaks from various ^{10,11}B(^{3}He,p$_x$)^{12,13}C reactions are visible. The prominent peak in channels around 300 originates from protons from the ^{11}B(^{3}He,p$_{8,9,10}$)^{13}C reactions. These peaks cannot be evaluated quantitatively due to lack of cross-section data. The peaks from ^{12}C(^{3}He,p$_0$)^{14}N, ^{12}C(^{3}He,p$_1$)^{14}N, ^{16}O(^{3}He,p$_0$)^{18}F and ^{12}C(^{3}He,p$_2$)^{14}N reactions are also visible. The peaks from the ^{12}C(^{3}He,p$_1$)^{14}N and ^{16}O(^{3}He,p$_0$)^{18}F reactions partly overlap at this incident energy in channels around 170.

curvature. Erosion by ions typically results in a directional erosion with a higher erosion at the direction of ion impact, while erosion by CX neutral particles should result in a more uniform erosion. The relatively uniform distribution of boron on the inner wall tiles, see Figs. 5 and 6, therefore suggests, that erosion by incident ions on these tiles is small. Whether the variation of the amount of deposited boron on the different tiles is due to a variation of the amount of boron deposited during boronisations, or is due to different erosion by variations of CX fluxes or energies, cannot be derived from the present data but requires further investigations.

3.2. Individual boronisations in OP 2.1

The samples exposed during individual boronisations were analyzed using NRA with 3 MeV ^{3}He ions, see section 2.2.2. The amounts of boron, carbon and oxygen deposited during 2 individual boronisations in OP 2.1 on different material samples exposed with the MPM are shown in Fig. 7. The 'C polished', Al and W samples had polished surfaces, while the 'C unpolished' sample had a grinded surface. The Cu sample has been electro polished, but showed also a rough surface. During the boronisation on 4.2.2023 100 – 150 × 10^{15} B-atoms/cm^2 (about 10 – 15 nm) have been deposited on the samples. The different samples show some variation of layer thickness, however, these variations are not systematic. There is no observable systematic dependence of the amount of boron with the mass of substrate material (C - Al - Cu - W), and there is no systematic dependence on surface roughness (polished and unpolished C; rough Cu). This suggests, that the thickness of boronisation layers on the different surfaces inside W7-X (fine grain graphite tiles, stainless steel panels, tungsten-coated tiles) shows also only a weak material dependence within less than 50 %.

The amount of carbon is about 20 × 10^{15} C-atoms/cm^2 (about 2 nm) on all samples and for both boronisations. This amount of carbon is typical for samples which have been exposed to air. The observed carbon may originate from air exposure, but carbon deposition during the boronisation cannot be excluded.

Protons from the ^{12}C(^{3}He,p$_1$)^{14}N and ^{16}O(^{3}He,p$_0$)^{18}F reactions partly overlap, see Fig. 4. This is not a problem for oxygen detection in thin layers, because the cross-section of the ^{12}C(^{3}He,p$_1$)^{14}N is small compared to the ^{16}O(^{3}He,p$_0$)^{18}F cross-section and the peaks are narrow enough to be separated. However, for the bulk carbon samples the overlap of both peaks cannot be disentangled, and oxygen therefore cannot be measured on bulk carbon samples. The layers contain substantial amounts of oxygen, with a ratio O/B of 0.5 – 0.6 for the boronisation on 4.2.2023 and a ratio O/B of 0.8 – 0.9 for the boronisation on 25.2.2023. As the layers have been exposed to air prior to analysis, the oxygen most probably originates from the air exposure. Nevertheless, the amount of trapped oxygen allows to estimate the oxygen gettering capacity of the boronisation layers, which is therefore up to 0.5 - 0.9O/B. Assuming a total boronized surface area inside W7-X of 192.5 m^2 [14], a typical boronization layer thickness of 100 × 10^{15} B-atoms/cm^2 (about 10 nm), and an oxygen gettering capacity of 0.5 - 0.9 O/B, this gives an oxygen gettering capacity of an individual boronisation of about 10^{23} – 2 × 10^{23}O-atoms (about 2.6 – 5.2 g oxygen). This is relatively large despite the small thickness due to the large active wall area.

In addition, the layers contain hydrogen. The amount of hydrogen has not been determined, but is difficult to interpret as it might originate from the boronisation, but might as well originate from trapping of water during exposure to moist air.

The most striking difference between the layers deposited during the boronisations on 4.2.2023 and on 25.2.2023 are their different thickness: While on 4.2.2023 100 – 150 × 10^{15} B-atoms/cm^2 (10 – 15 nm) were deposited, only 50 – 70 × 10^{15} B-atoms/cm^2(5 – 7 nm) have been deposited on 25.2.2023. The boronisation on 4.2.2023 lasted 2:26 h at a pressure of 9 – 11 × 10^{-3} mbar with an injected gas amount of 35.4 bar*l. The boronisation on 25.2.2023 lasted 3:10 h at a pressure of 8 × 10^{-3} mbar with an injected gas amount of 38.1 bar*l. I.e., these parameters are comparable for both boronisations and do not explain the different layer thicknesses. The main difference between both boronisations was the electrode current, which was 1 – 1.7 Ampere on 4.2.2023, but only about 0.8 Ampere on 25.2.2023. This is reasonable, as in a zero-order model the deposited layer thickness should be proportional to the time-integrated discharge current. It therefore can be concluded as engineering rule of thumb, that 1 A × h (Ampere times hour) of boronisation results in a boronisation layer with a thickness of about 30 × 10^{15} B-atoms/cm^2 (about 3 nm) at the position of the MPM. The accuracy of this rule of thumb is about 50 %.

As there is only one manipulator available for sample exposure during individual boronisations, direct measurements of the lateral inhomogeneity of the boron layer thickness distribution are not possible. As described in section 3.1, as result of three boronisations in OP 1.2b 100 – 600 × 10^{15} B-atoms/cm^2 (about 10—60 nm) were found after the campaign. This is in good agreement with 50 – 150 × 10^{15} B-atoms/cm^2 (5 – 15 nm) for an individual boronisation in OP 2.1 at the position of the MPM.

4. Conclusions

Boronisations proved to be a key point for substantially reducing the plasma impurity content in W7-X, thus enabling successful plasma operation. The first three boronisations were performed during the operational period OP 1.2b, followed by five boronisations in the operational period OP 2.1. After OP 1.2b, deposited layers were observed on all inner surfaces. Campaign-integrated deposited layers were analyzed on 21 inner wall tiles using ion beam analysis methods. Most layers consisted mostly of boron with additional carbon and oxygen.

In OP 2.1, different materials were exposed during two individual

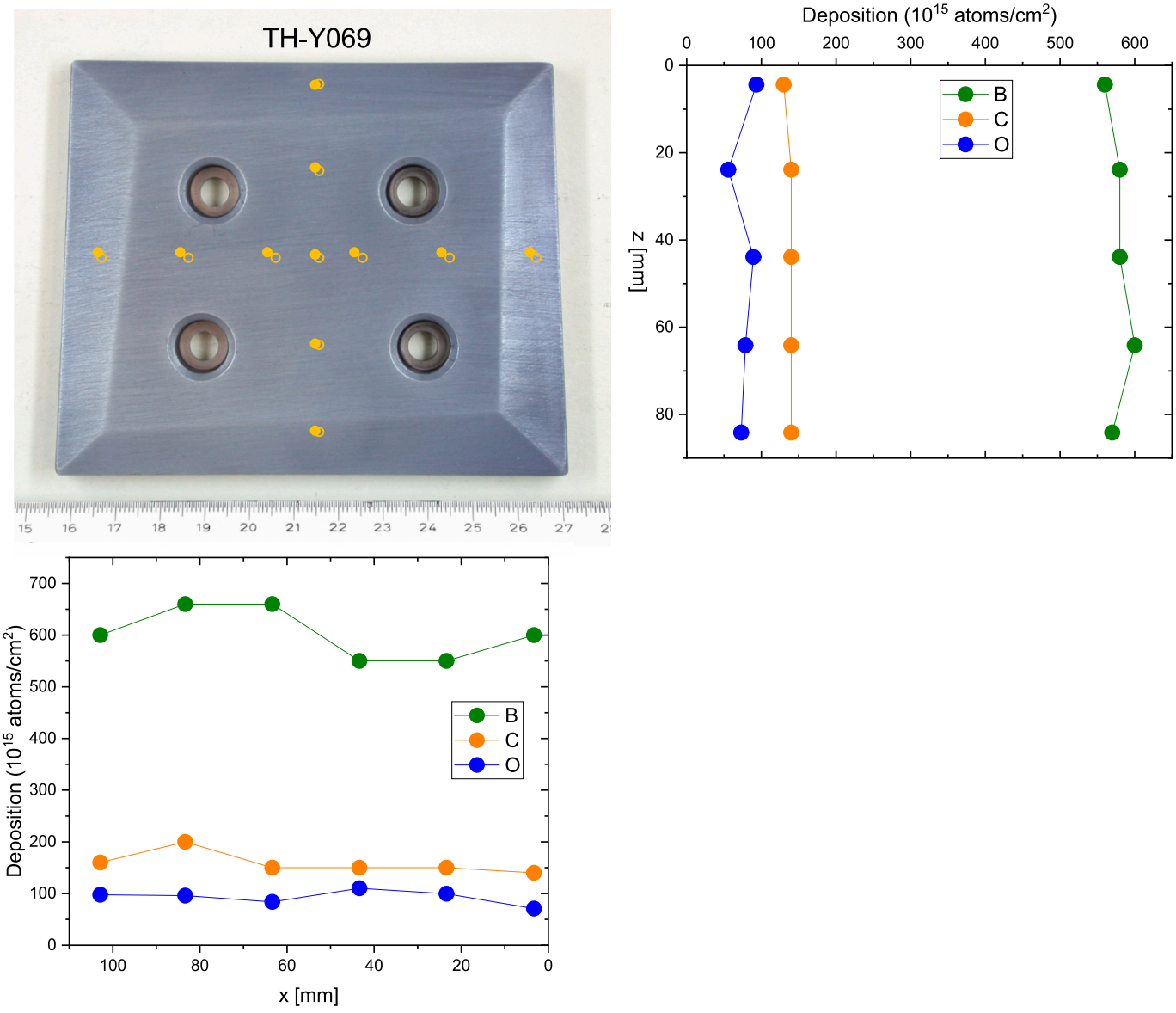

Fig. 5. Example of a W-coated inner-wall tile with a thicker boron layer after OP 1.2b. Tile TH-Y069, module 4, Abschirmhaus (see Fig. 1). Upper left: Photo of the tile. Full circles: Measurement points before exposure; open circles: Measurement points after exposure. A backscattering spectrum from the measurement point in the middle of the tile is shown in Fig. 2. Upper right: Amounts of B, C and O in the deposited layer on the tile after exposure in vertical direction in the middle of the tile; Lower left: Amounts of B, C and O in the deposited layer on the tile after exposure in horizontal direction in the middle of the tile.

boronisations using the multi-purpose manipulator, deposited boronisation layers on the samples were analyzed using nuclear reaction analysis. The layers contained 50 – 150 $\times$ 10^{15} B-atoms/cm^2 (5 – 15 nm), which is relatively thin. Deposited layer thicknesses showed some variation depending on substrate material and surface roughness, but a systematic dependence on material and/or roughness was not observed. Under the typical boronisation conditions at W7-X, one A $\times$ h of boronisation results in a boronisation layer with a thickness of about 30 $\pm$ 15 $\times$ 10^{15} B-atoms/cm^2 (about 3 $\pm$ 1.5 nm) at the position of the MPM.

The oxygen gettering capacity of the layers is up to 0.5 - 0.9O/B. The oxygen gettering capacity of an individual boronisation can be estimated to be about 10^{23} – 2 $\times$ 10^{23}O-atoms (about 2.7 – 5.4 g oxygen), which is relatively large despite the small layer thickness due to the large wall area covered by boronisations.

Boronisation layers are eroded either by ion impact (in areas with direct plasma contact) or due to erosion by charge-exchange (CX) neutral particles. The life time of such thin layers in areas with ion impact is expected to be small, and redeposition of boron together with carbon was already observed at the TDU. However, the life time in recessed areas without direct plasma contact and erosion by CX-neutrals only seems to be sufficiently long to prevent the necessity of too frequent boronisations.

CRediT authorship contribution statement

M. Mayer: Writing – review & editing, Writing – original draft, Validation, Project administration, Methodology, Investigation, Formal analysis, Conceptualization. **M. Balden:** Investigation. **T. Bräuer:** Investigation. **D. Cipciar:** Investigation. **C.P. Dhard:** Writing – review & editing, Investigation. **P. Drews:** Investigation. **S. Elgeti:** Investigation, Conceptualization. **D. Höschen:** Investigation. **C. Killer:** Investigation. **D. Naujoks:** . **N. Sandri:** Investigation. **J.-H. Schmid-Dencker:** Visualization, Investigation, Formal analysis. **L. Vanó:** Writing – review & editing, Investigation. **H. Viebke:** Investigation. **O. Volzke:** Investigation.

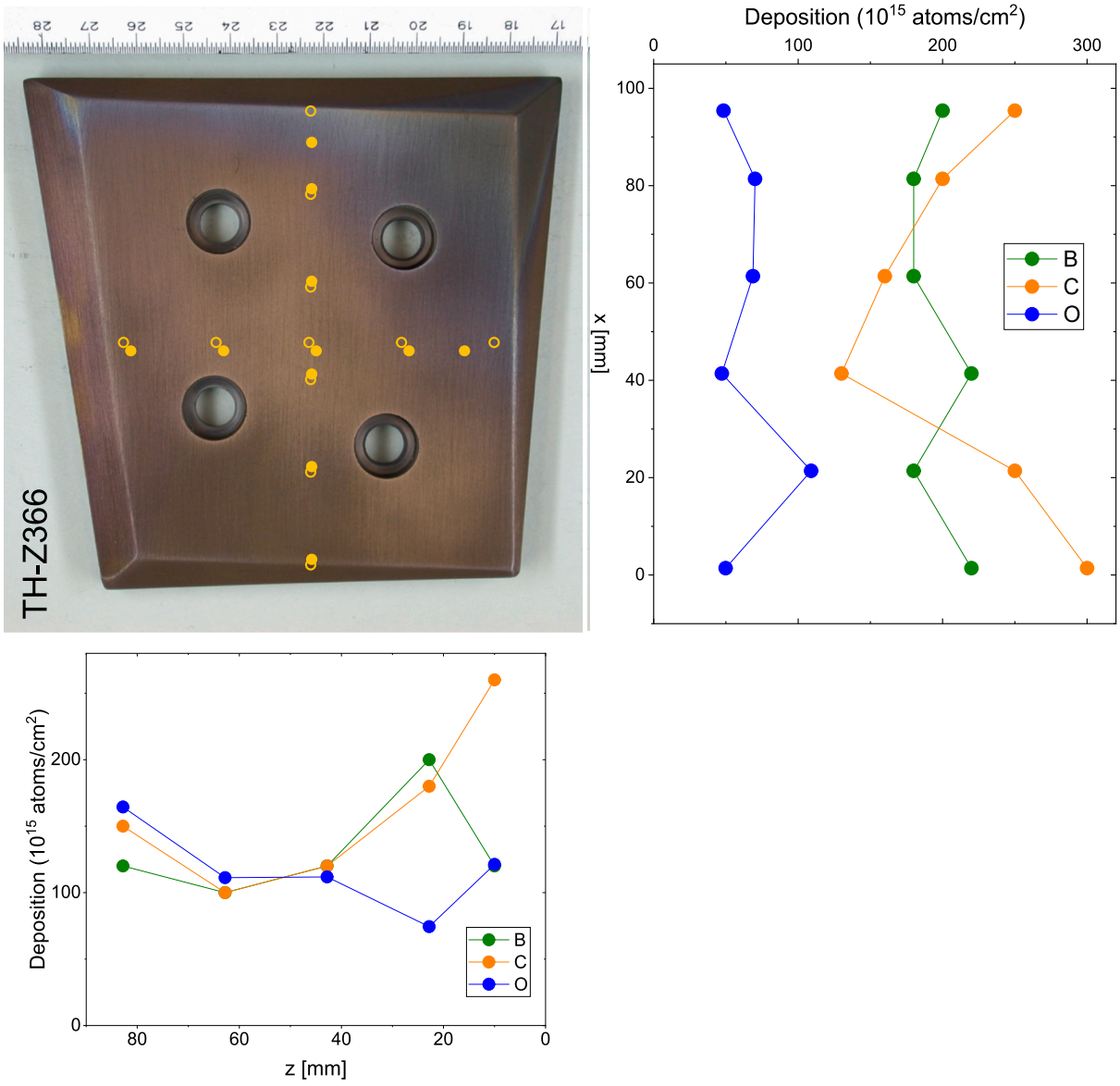

Fig. 6. Example of a W-coated inner-wall tile with a thinner and more carbon-rich boron layer after OP 1.2b. Tile TH-Z366, module 2, see Fig. 1. The orientation of the tile is identical to Fig. 1. Upper left: Photo of the tile after exposure in OP 1.2b. Full circles: Measurement points before exposure; open circles: Measurement points after exposure. Upper right: Amounts of B, C and O in the deposited layer on the tile after exposure in vertical direction in the middle of the tile; Lower left: Amounts of B, C and O in the deposited layer on the tile after exposure in horizontal direction in the middle of the tile.

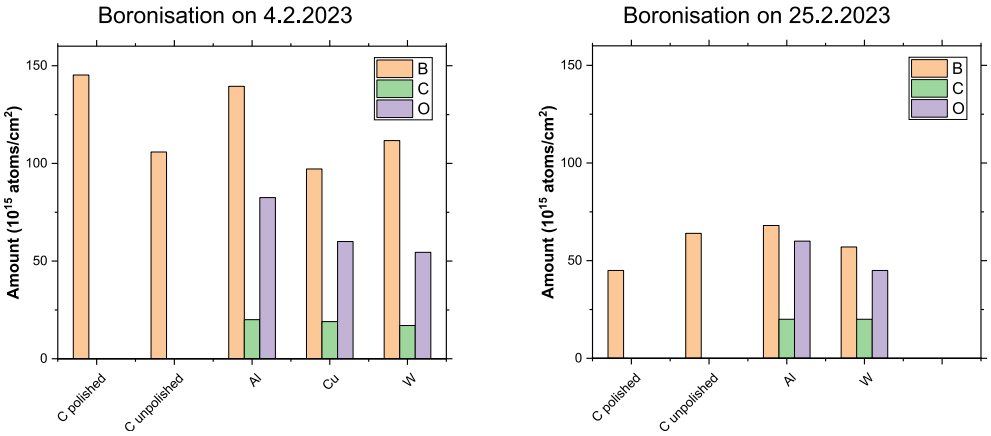

Fig. 7. Amounts of boron, carbon and oxygen on different materials exposed with the MPM during individual boronisations on 4.2.2023 and 25.2.2023.

Declaration of competing interest

The authors declare that they have no known competing financial interests or personal relationships that could have appeared to influence the work reported in this paper.

Acknowledgements

This work has been carried out within the framework of the EUROfusion Consortium, funded by the European Union via the Euratom Research and Training Programme (Grant Agreement No 101052200 — EUROfusion). Views and opinions expressed are however those of the author(s) only and do not necessarily reflect those of the European Union or the European Commission. Neither the European Union nor the European Commission can be held responsible for them.

Data availability

Data will be made available on request.

References

[1] C. Beidler, et al., Physics and Engineering Design for Wendelstein VII-X, Fusion Technol. 17 (1990) 148.
[2] R.C. Wolf, et al., Major Results from the First Plasma Campaign of the Wendelstein 7-X Stellarator, Nucl. Fusion 57 (2017) 102020.
[3] H.-S. Bosch, et al., Final Integration, Commissioning and Start of the Wendelstein 7-X Stellarator Operation, Nucl. Fusion 57 (2017) 116015.
[4] T. Sunn Pedersen, et al., Key Results from the First Plasma Operation Phase and Outlook for Future Performance in Wendelstein 7-X, Phys. Plasmas 24 (2017) 055503.
[5] C.D. Beidler, et al., Demonstration of reduced neoclassical energy transport in Wendelstein 7-X, Nature 596 (2021) 221.
[6] T. Sunn Pedersen, et al., Experimental confirmation of efficient island divertor operation and successful neoclassical transport optimization in Wendelstein 7-X, Nucl. Fusion 62 (2022) 042022.
[7] A. Peacock, et al., Progress in the Design and Development of a Test Divertor (TDU) for the Start of W7-X Operation, Fusion Eng. Des. 84 (2009) 1475.
[8] T. Sunn Pedersen, et al., First Results from Divertor Operation in Wendelstein 7-X, Plasma Phys. Controlled Fusion 61 (2019) 014035.
[9] A. Goriaev, T. Wauters, R. Brakel, S. Brezinsek, A. Dinklage, J. Fellinger, H. Grote, D. Moseev, S. Sereda, O Volzke and W7-X team, Wall conditioning at the Wendelstein 7-X stellarator operating with a graphite divertor, Phys. Scr. T171 (2020) 014063.
[10] S. Sereda, et al., Impact of boronizations on impurity sources and performance in Wendelstein 7-X, Nucl. Fusion 60 (2020) 086007.
[11] M. Mayer, M. Kandler, C.P. Dhard, S. Elgeti, Y. Gao, M. Jakubowski, D. Naujoks, L. Rudischhauser, W7-X Team, Assessment of carbon net erosion/deposition at the divertor of W7-X, Nucl. Mater. Energy 34 (2023) 101352.
[12] E. Wang, et al., Impurity sources and fluxes in W7-X: from the plasma-facing components to the edge layer, Phys. Scr. T171 (2020) 014040.
[13] A. Goriaev, Study and Optimisation of Wall Conditioning Methods on the Superconducting Stellarator W7-X, PhD thesis, Ghent University, Ghent, Belgium, Feb. 2022, http://hdl.handle.net/1854/LU-8744665.
[14] C.P. Dhard, et al., Plasma-wall interaction studies in W7-X: main results from the recent divertor operations, Phys. Scr. 96 (2021) 124059.
[15] M. Mayer, et al., Erosion of tungsten marker layers in W7-X, Phys. Scr. 96 (2021) 124070.
[16] C.R. Gossett, Non-Rutherford elastic backscattering for light element cross section enhancement, Nucl. Instr. Meth. B40/41 (1989) 813.
[17] M. Mayer, et al., Ion beam analysis of fusion plasma-facing materials and components: facilities and research challenges Nucl, Fusion 60 (2020) 025001.
[18] M. Mayer, Improved Physics in SIMNRA 7, Nucl. Instrum. Methods Phys. Res. B 332 (2014) 176.
[19] J.F. Ziegler, SRIM-2003, Nucl. Instrum. Methods Phys. Res. B 219–220 (2004) 1027.
[20] A.F. Gurbich, SigmaCalc recent development and present status of the evaluated cross-sections for IBA, Nucl. Instrum. Methods Phys. Res. B 371 (2016) 27.
[21] G. Vizkelethy, Nuclear reaction analysis: Particle-particle reactions, in: J. R. Tesmer, M. Nastasi (Eds.), Handbook of Modern Ion Beam Materials Analysis, Materials Research Society, Pittsburgh, 1995.
[22] L.C. McIntyre Jr., J.A. Leavitt, M.D. Ashbaugh, J. Borgardt, E. Andrade, J. Rickards, A. Oliver, Cross section measurements for the (3He, p) nuclear reaction on B and N between 2 and 4 MeV, Nucl. Instrum. Methods Phys. Res. B 118 (1996) 219.
[23] L. Hess, M. Mayer, T. Schwarz-Selinger, Cross-section data for the reactions 12C (3He, p0)14N to 12C(3He, p6)14N at energies up to 6 MeV, Nucl. Instrum. Methods Phys. Res. B 547 (2024) 165141.
[24] M. Guitart Corominas, T. Schwarz-Selinger, Experimental determination of the 16O (3He,p0)18F differential cross section, Nuclear Inst. and Methods in Physics Research B 450 (2019) 13.
[25] M. Mayer, E. Gauthier, K. Sugiyama, U. von Toussaint, Quantitative depth profiling of deuterium up to very large depths, Nucl. Instrum. Meth. Phys. Res. B 267 (2009) 506.
[26] G. Motojima, S. Masuzaki, C.P. Dhard, M. Krause, D. Naujoks, Y. Hayashi, S., Brezinsek and the W7-X Team, In-vessel colorimetry of Wendelstein 7-X first wall components: variation of layer deposition distribution in OP1.2a and OP1.2b, Phys. Scr. T171 (2020) 014054.
[27] M. Mayer, et al., Carbon erosion/deposition on the divertor of W7-X during the operational period OP 1.2b, Nuclear Fusion 62 (2022) 126049.